Fusion and Quasi-El..''c processes near the Coulomb Barrier.

Daniel Abriola

Departamento de Fisica, Tandar, Comisión Nacional de Energia Atómica. Avda del Libertador 8250

1429 Buenos Aires Argentina.

1. Introduction

The enhancement of the fusion cross section below the Coulomb Barrier has been the subject of great theoretical and experimental interest[1),2)]. This work presents an overview of the phenomenon and of current theoretical descriptions, emphasizing the relations with direct reactions.

Section 2 presents the definition and systematic behaviour of the fusion enhancement below the Coulomb Barrier (CB). Section 3 shows the rôle of coupling to surface degrees of freedom, namely permanent deformations of nuclei, inelastic and transfer channels. Section 4 points out the importance of studies describing simultaneously quasi-elastic processes and fusion. Finally concluding remarks are presented in section 5.

2. Systematic of fusion enhancement below the barrier

The fusion cross section is given clasically by:

$$\sigma_f = \begin{cases} \pi R_B^2 (1 - V_B/E) & \text{for } E > V_B \\ 0 & \text{for } E \leq V_B \end{cases} \qquad (1)$$

where V_B is the Barrier height , R_B its radius (see Fig.1), and $V_l(r)$ is the effective potential:

$$V_l(r) = V_N(r) + V_C(r) + l(l+1)\hbar^2/2\mu r^2 \qquad (2)$$

Considering quantum-mechanical barrier penetration one has:

$$\sigma_f = \pi \lambda^2 \sum_{l=0}^{\infty} (2l+1)\, T_l \qquad (3)$$

The transmition coeficients T_l might be evaluated directly solving the Schrödinger equations or by making use of the WKB approximations i.e.

$$T_l(E) = 1 / (1 + \exp S_l(E)) \qquad (4)$$

and

$$S_l(E) = (8\mu/\hbar^2)^{1/2} \int_{r_i}^{r_0} (V_l(r)-E)^{1/2}\, dr \qquad (5)$$

The one-dimensional barrier penetration model, used with an energy-independent nuclear potential $V_n(r)$ that adjust the fusion cross sections above the barrier performs nicely for light heavy ions . On the other hand, for $200 < Z1.Z2 < 1100$ there is a systemat.c enhancement of the fusion cross section data below the barrier with respect to one dimensional barrier penetration calculations.

In an attempt to study the systematic behaviour of the fusion enhancement Vaz el al[3] have parametrized the transmition coeficients in terms of Wong's model:

$$T_l = 1 / (1 + \exp(2\pi(V_l(R_l)-E)/\hbar\omega_l)) \qquad (6)$$

with

$$\hbar\omega_l = [\hbar^2/\mu \; d^2V(r,l)/dr^2|_{Rl}\,]^{1/2} \qquad (7)$$

where R_l, $V_l(R_l)$ (given by (2)), and $\hbar\omega_l$ are the position, height and curvature af the barrier, for the l^{th}-wave.
They adjusted V_n to fit the fusion data above the CB and introduced an energy-dependent parameter ΔR to be added to the nuclear radius. They fitted all the fusion data available and obtained a systematic increase of ΔR with decreasing energies as presented in Fig.2. They conclude that there is an enhancement of the nuclear attraction (or dynamic nuclear polarization) that is a general phenomenon in subbarrier fusion.

There are, however pronounced differences between isotopes that point out the relevance of the intrinsic degrees of freedom as it is reviewed in the next section.

3. Intrinsic degrees of freedom

3.1 Static deformation

The fusion cross sections migth be enhanced due to a lowering of the CB caused by static deformation of the target. This effect has been studied in Ref 4) and more recently in Ref 5). It arises from the gain in fusion probability due to a lowering of the CB in a collision with a prolate nucleus having the deformation axis parallel to the beam direction (see Fig.3). In Ref.5 the fusion of ^{16}O plus the spherical ^{144}Sm is the starting ground to find a "basic" or "bare" barrier over which the inclusion of the deformation of the other Sm isotopes by means of Wong's model suffices to fit their fusion cross section data (see Fig 4). Therefore, in the $^{16}O + ^{A}Sm$ system, the simple static deformation of the target describes the subbarrier fusion; a similar conclusion is found, in Ref.2 for the system $^{40}Ar + ^{A}Sm$.

3.2 Vibrations

The effect of coupling to surface excitations might be schematically studied by means of radius fluctuations due to zero point motion (ZPM): the system radius R= R1 + R2 fluctuates due to surface excitations given by the standard deviation $\sigma_\lambda(R1+R2)$ which is related to the B(Eλ) value of the excited state by[2]:

$$\sigma_\lambda = [R/Z(\lambda+3)]\,[(2\lambda+1)\,B(E\lambda)]^{1/2} \qquad (8)$$

where B(Eλ) is in W.U. Within the framework of this model, Reisdorf et al[6] measured fusion in ^{40}Ar + Sn and ^{40}Ar + Sm and removed the trivial geometric effects in the different isotopes by scaling the energies and cross sections as:

$$\sigma_f^* = \sigma_f\,(R_B^o/R_B)^2 \quad \text{and} \quad E_{cm}^* = E_{cm}\,(V_B^o/V_B) \qquad (9)$$

where R_B^o and V_B^o are the possition and height of the barrier

for the reference system. They used a nuclear potential given by:

$$V(s) = V_N R_{12} \exp(-s/d) \quad (10)$$

where $s = R-(R1+R2)$ (11)

and $R12 = R1\ R2 / R1+R2$ (12)

A fluctuation in the system radius $\sigma(R1+R2)$ will produce a fluctuation of the barrier $\sigma(V_B)$. The effect of adjusting $\sigma(R1+R2)$ and V_B is shown in Fig. 4. The zero point fluctuations found were in agreement with the values expected from the theoretical values extracted from the known B(E2) values.

This model, however, assumes that all levels are degenerate. This is a reasonable assumption for rotations where the mean excitation energy is small compared to $\hbar\omega$, but is not the general case for vibrations. A more exact way to asses the influence of the vibrational degrees of freedom is to perform Coupled Channels Calculations (CCC).

The coupled channels equations:

$$[d^2/dr^2 - l_\alpha(l_\alpha+1)/r^2 - V_\alpha^{opt} + K_\alpha^2]\ R_\alpha^{J\pi}(r) = \sum_\beta V_{\alpha\beta} R_\beta^{J\pi}(r) \quad (13)$$

are solved with a CCC computer code and the fusion cross section is evaluated from:

$$\sigma_{reac} = \sigma_{inel} + \sigma_f = \pi\lambda^2 \sum_{l\alpha} (2l_\alpha+1)\,(1-|S_l^\alpha(E)|^2) \quad (14)$$

where $S_l(E)$ is the coupled channels S-matrix.

An example of CCC is the analysis of fusion in $^{32}S + ^{24,28}Mg$ performed in Ref 7. where a good agreement with the experimental data is obtained by using a "bare" potential taken from systematics (the Akyuz-Winther potential) plus a coupling the first excited states in both projectile and target (see Fig. 8).

3.3 Transfer degrees of freedom

Still another way to enhance fusion is the coupling of the relative motion to transfer channels with positive effective Q-values. In fact those reactions increase the kinetic energy in the outgoing channel thus easing the tunnelling throught the barrier. An example of such an effect is seen in Fig.7 where the fusion data [8] of different isotopes of Ni + Ni are displayed. One can see in the reduced plot that the channel that presents a positive Q-value is enhanced at low energies by a factor of around 20 .

Dasso et al[9] have shown, making use of a schematic coupling model, that coupling to negative Q-values channels (either transfer or inelastic) also enhances the fusion cross section.

Naively it is expected that if a particular transfer channel is an important doorway to fusion, the cross section of that direct reaction channel should be relatively important. In fact for the previosly mentioned system of the Ni isotopes this seems to be the case as might be seen in Fig.8. Here the 1n pickup is enhanced in the $^{58}Ni + ^{64}Ni$ system as it is the fusion cross section.

Another argument in favour of such correlation is presented by Rehm[10] . He shows that there is a correlation between the zero-point fluctuation needed to explain the observed enhancements in several systems, with the cross section for neutron transfer (sum of stripping and pickup); this is shown in Fig. 9.

The relative importance of coupling to transfer channels with positive Q-value to the coupling to strong transfer channels regardeless of Q has been addressed by Henning et al[11] using a schemmatic two channels coupling model. It is shown that: a) if the coupling strength between the channels

is constant as a function of Q-value, the fusion enhancement factor increases for positive Q-values, b) if the transfer cross section is constant as a function of Q-value the enhancenent is large for large negative and positive Q-values and c) in a more realistic case, if the transfer cross sections have a bell shape centered arround a Q-optimum, the enhancement factor has also a bell shape centered arround Q-optimum. Such calculations are displayed in Fig.10.

4. Simultaneous description of Quasi-Elastic and fusion processes.

The first attempt to simultaneously describe elastic, inelastic, transfer and fusion processes was performed in 1985 by Pieper et al[12]. It was a coupled channel calculation for the ^{16}O + ^{208}Pb system, with a potential chosen to describe the elastic channel. Simplifications were made to evaluate the coupling to the transfer channels. The results are in general agreement with the data although several discrepencies remain as seen in Fig.11.

An alternative to the complicated and sometimes unmanageable coupled channels approach, at least regarding the elastic and fusion reactions, is the use of the dispersion relations which correlate the real and imaginary parts of the optical potentials. In fact Mahaux et al[13] have shown that near the Couiomb Barrier the imaginary potential should decrease with decreasing energy due to the closing of the reaction channels, the dispersion relation change, in turn the real potential as a function of the energy. Fig 12 shows the values of the real and imaginary potentials for the ^{16}O + ^{208}Pb system which describe the elastic data at different energies. The solid lines are calculations performed with the schemmatic form of the dispersion relations:

$$V_{Rs} = V_0 + \Delta V(E) \qquad (15)$$

with

$$\Delta V(E) = W_0/\pi \left[\varepsilon_a \ln|\varepsilon_a| - \varepsilon_b \ln|\varepsilon_b|\right] \quad (16)$$

where

$$\varepsilon_i = E-E_i/E_b-E_a \quad (17)$$

E_a, E_b, and W_0 are indicated in Fig.12-a). When the real part of such a potential is used together with a short range imaginary potential [13,7] the fusion cross section results in good agreement with the data (see Fig.12 b)).

In the Tandar Laboratory at Buenos Aires the elastic, inelastic[14] and transfer scattering[15] have been measured for the $^{16}O + ^{144}Sm$ system. Fig.13 shows the best adjustements to the data obtained with energy-independent potentials, whose parameters are shown in Table 1 .

Table 1

Values of χ^2/point.

Potentials RP1 : V=193 MeV, r_0=1.33 fm, a=0.287 fm

RP2 : V=224.2 MeV, r_0=1.172 fm, a=0.8 fm

RP3 : V=102 MeV, r_0=1.27 fm, a=0.412 fm

CP2 : See Text.

Potential	Angular Distributions		Fusion
	72.3 MeV	69.2 MeV	
RP1	0.919	2.343	$3.1\ 10^4$
RP2	7.980	21.13	8.57
RP3	4.388	17.91	7.40
CP2	0.826	1.033	4.41

It is seen, comparing with the calculated fusion cross section displayed in Fig.14 that with energy-independent potentials is not possible to obtain a simultaneus adjustment of elastic and fusion data. On the other hand the energy

dependent potentials shown in Fig.15 allow a good simultaneus description of elastic and fusion data as migth be seen from the values of χ^2/point presented in Table 1. This approach should still be useful in coupled channels calculations since it should include in an average way the effect of truncation of the channel space.

5. Concluding remarks

The fusion enhancement below the Coulomb Barrier is correlated with static deformation of the nuclei and coupling to peripheral reactions. The direct reaction theory appears to account for the phenomenon, although still in a semi-quantitative way.

From the theoretical side more reliable CCC are needed with realistic treatment of the transfer channels (Fresco) and better adjustement of the Quasi-Elastic data . From the experimental point of view the measurement of detailed quasi-elastic scattering cross sections in the vecinity of the Coulomb Barrier for systems in which the fusion excitation function is known, is essential. Such measurements should provide a stringent test to energy-dependent potentials and to CCC; they are in progress in several laboratories, among others Legnaro (^{32}S + $^{58,64}Ni$), Sao Paulo (^{16}O + $^{63,65}Cu$), and Buenos Aires (^{16}O + $^{144, 148}Sm$).

References

1) S.G.Steadman, ed. Fusion Reactions below the Coulomb Barrier, Lecture Notes in Physics, Vol 219 (Heidelberg: Springer Verlag).

2) J.L.Durell et al, ed. Proceedings of the international Nuclear Physics Conference, Vol.2 Harrogate 1986 IOP publishing p.203.

3) P. Braun-Munzinger, ed. Nuclear Physics with Heavy Ions. Proceedings of the International Conference on Nuclear Physics with Heavy Ions. SUNY, at Stony Brook 1983 p. 31.

4) R. G. Stockstad and E. E. Gross, Phys. Rev C23 (1981), 281

5) D. DiGregorio et al, Phys Lett B176 (1986), 322

6) W. Reisdorf et al, Phys Rev Lett 49 (1982), 1811

7) M. Rhoades-Brown et al, Phys Lett B138 (1984), 19

8) M. Beckerman et al, Phys Rev Lett 45 (1980), 1472; Phys Rev C23 (1981), 1581 and Phys Rev C25 (1982), 837

9) C. H. Dasso et al, Nucl Phys A405 (1983), 381

10) K. E. Rehm. Influence of Quasi -Elastic Channels on Fusion, Argonne National Laboratory. PHY-4778-HI-88 (1988)

11) W. Henning et al, Phys Rev Lett 58 (1987), 318

12) S. C. Pieper et al, Phys Lett B162 (1985), 43

13) C. Mahaux et al, Nucl Phys A449 (1986), 354

14) D. Abriola et al, Proceedingr of the International Nuclear Physics Conference Vol. 1. Harrogate 1986

15) A. J. Pacheco et al, Ibid.

Figure Captions.

Fig. 1- Effective potentia, and Barrier Parameters

Fig. 2- Change in the nuclear radius needed to adjust the fusion cross sections.

Fig. 3- Barrier fluctuation due to different orientations in the collision of a spherical proyectile with a prolate target.

Fig. 4- Fusion cross sections for the system $^{16}O + {}^{A}Sm$. Solid curves are fits to the data using Wong's model. (Taken from Ref. 5)

Fig. 5- Fusion cross sections for the systems $^{40}Ar + {}^{122}Sn$ and $^{40}Ar + {}^{154}Sm$. Full curves are two parameter fits to the

data, described in the text, the dashed curves are calculations with the same nuclear potential, but without barrier fluctuations and static deformation. (Taken from Ref.6)

Fig.6- Calculations of the fusion cross sections for the systems $^{32}S + ^{26}Mg$ and $^{32}S + ^{24}Mg$. (Taken from Ref.7)

Fig.7- Fusion cross sections for the systems $^{58}Ni + ^{58}Ni$, $^{58}Ni + ^{64}Ni$, and $^{64}Ni + ^{64}Ni$. (Shown schemmaticaly in a reduced scale)

Fig.8- Comparison of the cross sections for fusion reactions and neutron transfer reactions in the systems $^{58}Ni + ^{58}Ni$ and $^{58}Ni + ^{64}Ni$. (Taken from Ref.10)

Fig.9- Amplitude af the ZPM σ_0(fm) necessary to describe the enhancement of the fusion cross sections ploted vs. one neutron transfer cross section. (Taken from Ref.10)

Fig.10-Subbarrier fusion enhancement factor, calculated in the two channel mixing limit as a function of the quasi-elastic reaction Q-value. (Taken from Ref. 11)

Fig.11-a) Elastic differential cross section for $^{16}O + ^{208}Pb$. Solid curves are CCC. Dotted curves are results with no couplings. b) Total cross sections for the $^{16}O + ^{208}Pb$ system. Solid curve and squares are fusion; dashed curve and crosses are total quasi-elastic; dash-dotted curve and dots are the (^{16}O, ^{15}N) reaction. The dotted curve is single channel fusion. (Taken from Ref.12)

Fig.12-a) Dispersive corrections for $^{16}O + ^{208}Pb$. The potentials are evaluated at R_s=12.4 fm. b) Fusion cross sections. Solid line is a calculation using a barrier penetration model with the real potential shown in a). (Taken from Ref.13)

Fig.13-Elastic scattering for the system $^{16}O + ^{144}Sm$ at E_{lab}= 69.2 MeV and 72.3 MeV. Lines are Optical Model fits with the potentials displayed in Table 1.

Fig.14-Fusion cross sections for the system $^{16}O + ^{144}Sm$. The line have the same meaning as in Fig.13.

Fig.15-Dispersive corrections for $^{16}O + ^{144}Sm$. The potentials are evaluated at R_s= 11.8 fm.

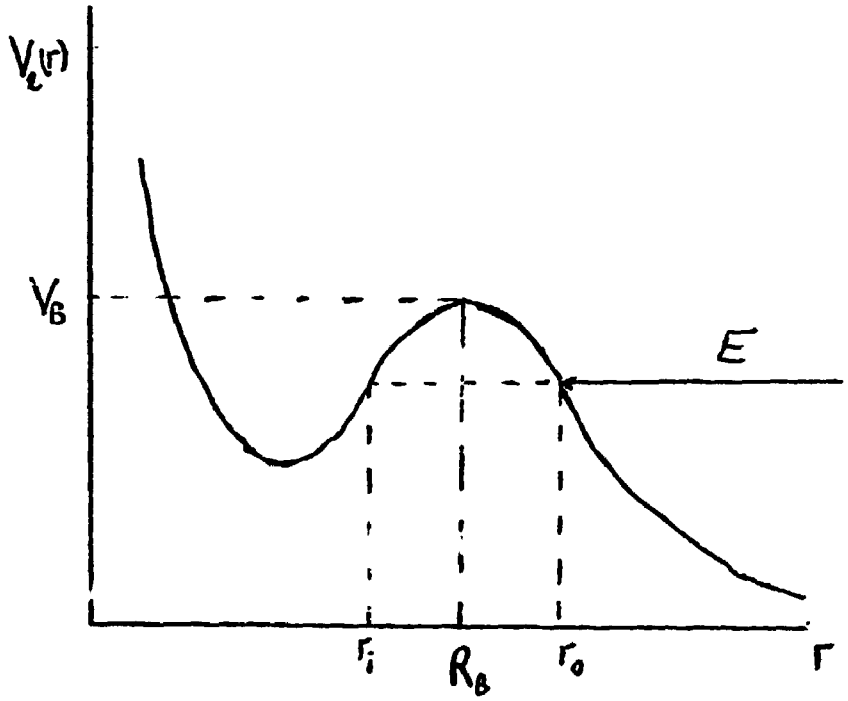

Fig. 1

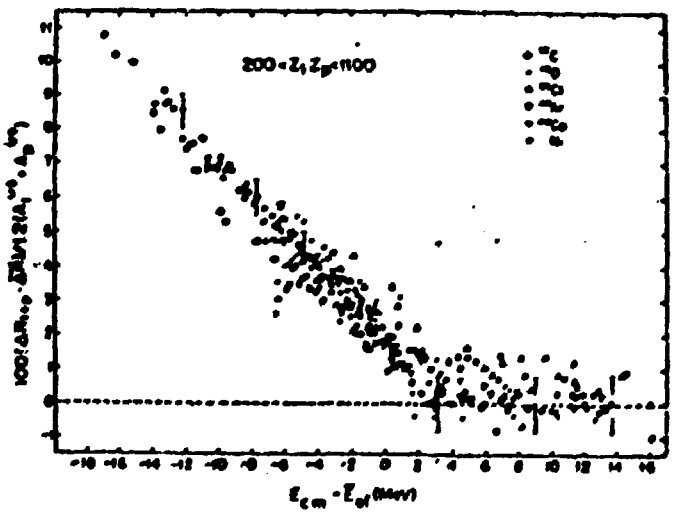

Fig. 2

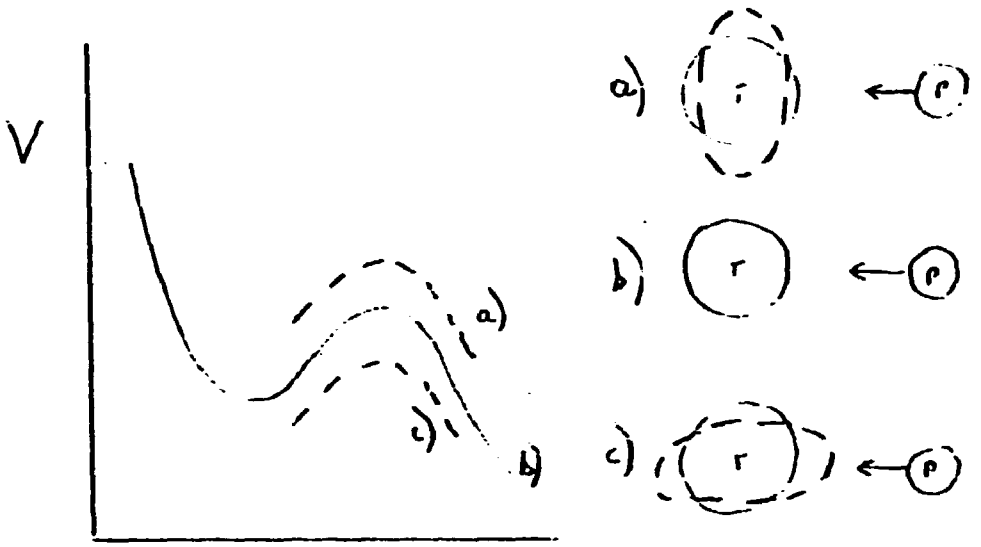
V
a)
b)
c)
a)
r
r
b)
r
r
c)
r
r

Fig. 3

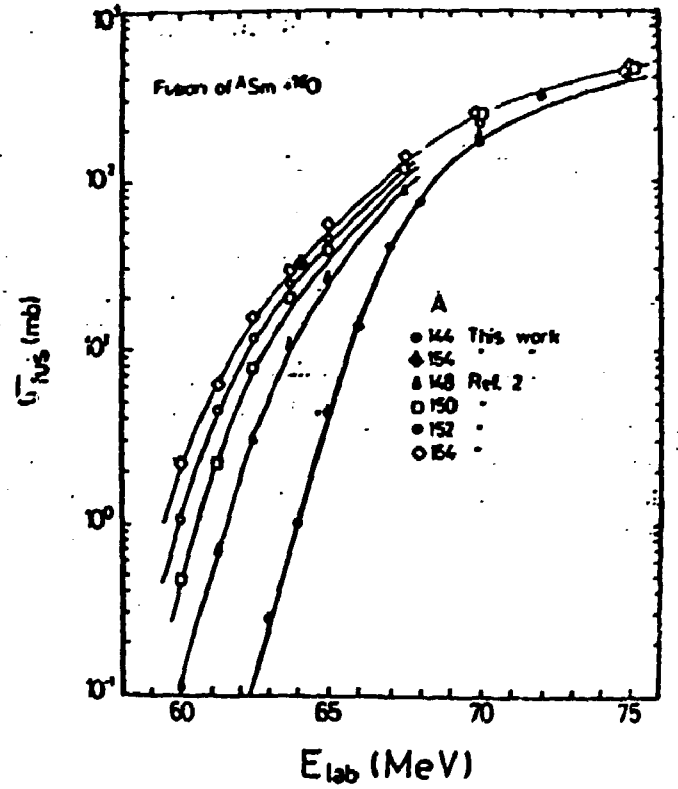
Fusion of ASm + 16O
A
144 This work
154
148 Ref. 2
150
152
154
60
65
70
75
E lab (MeV)

Fig. 4

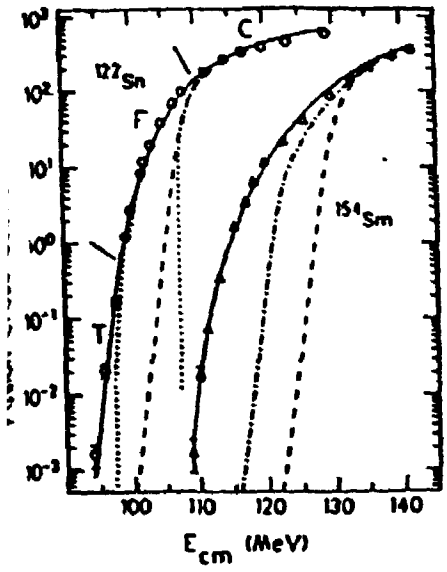

Fig. 5

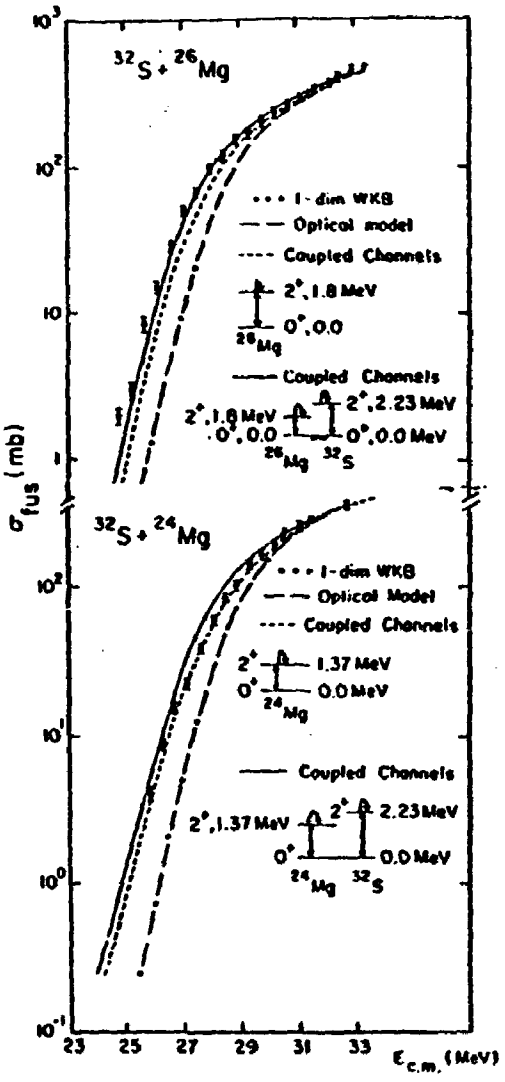

Fig. 6

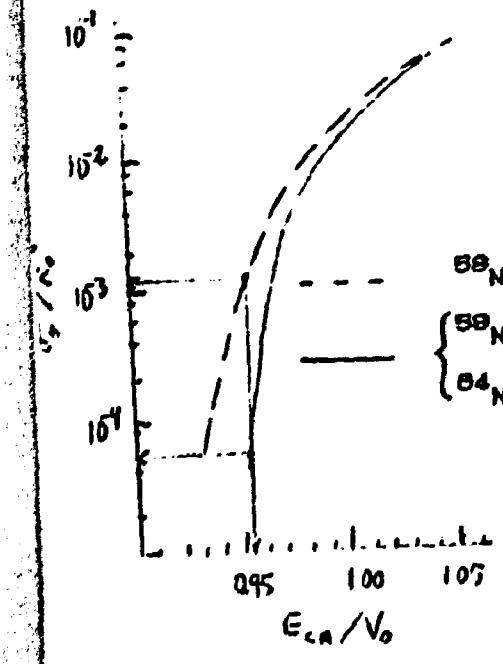

	Q_{g-g} [MeV] 1n	2n
^{68}Ni + ^{64}Ni	-0.8	+3.9
^{68}Ni + ^{68}Ni	-3.2	-2.1
^{64}Ni + ^{64}Ni	-3.6	-1.4

Fig. 7

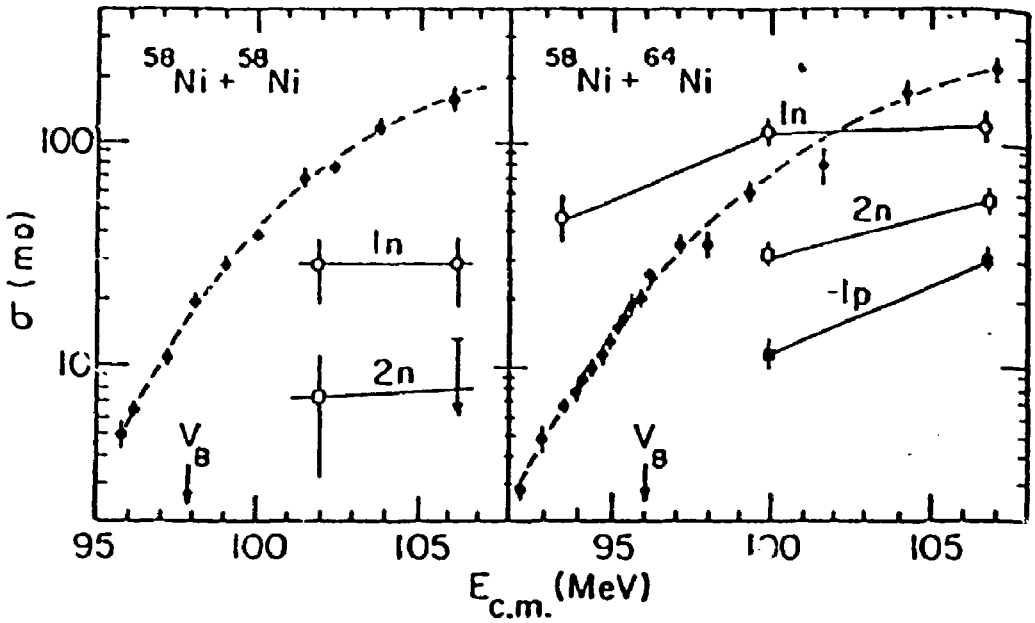
58Ni + 58Ni
58Ni + 64Ni
1n
2n
-1p
V_B
100
10
σ (mb)
95
100
105
E_c.m. (MeV)

Fig. 8

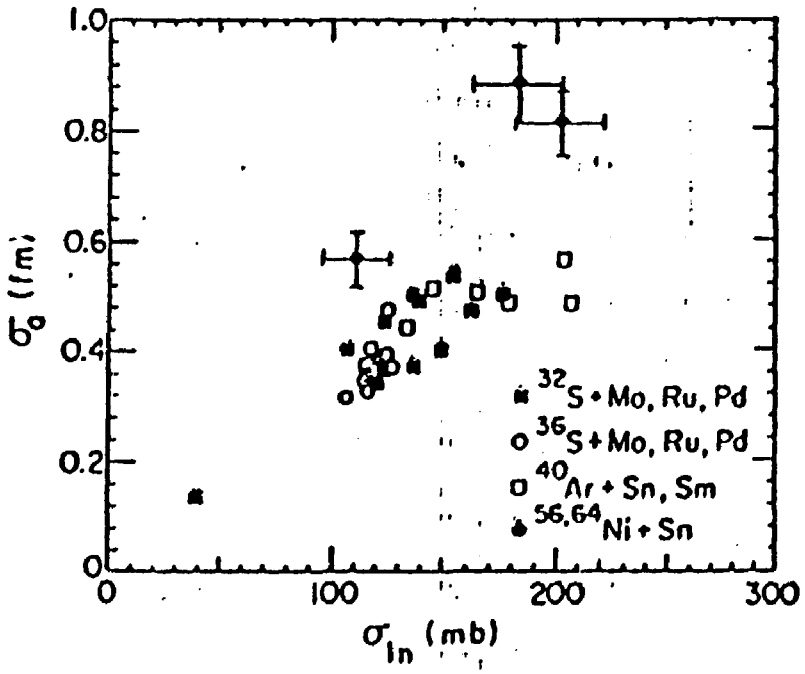
1.0
0.8
0.6
0.4
0.2
0
σ_0 (fm)
0
100
200
300
σ_1n (mb)
32S + Mo, Ru, Pd
36S + Mo, Ru, Pd
40Ar + Sn, Sm
56,64Ni + Sn

Fig. 9

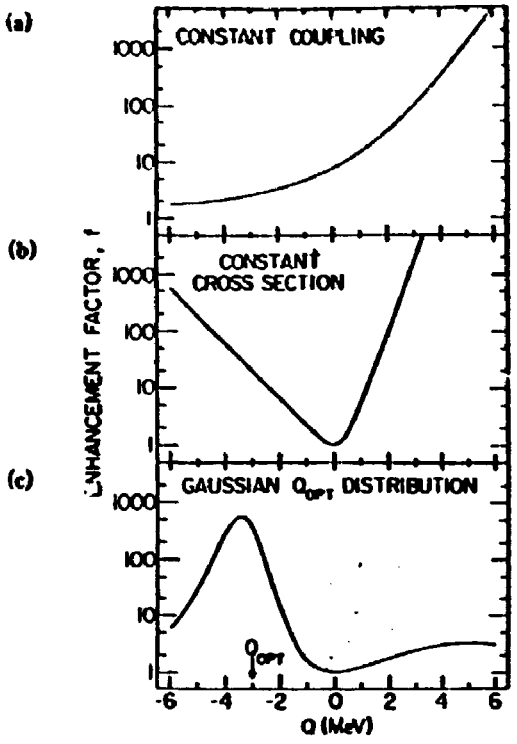

Fig. 10

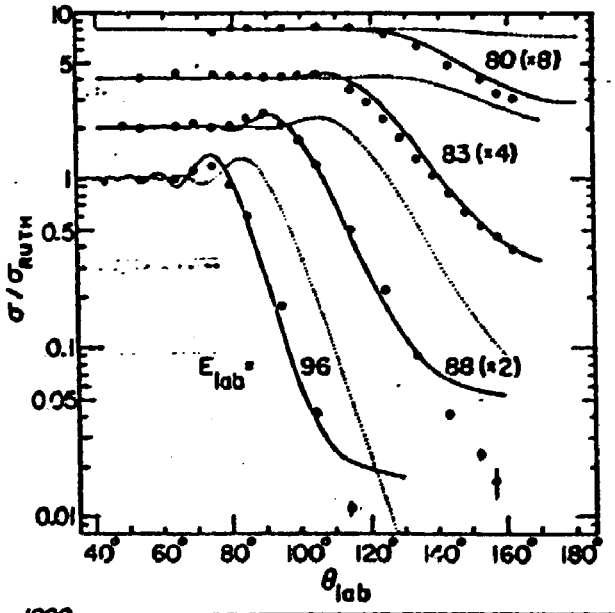

a)

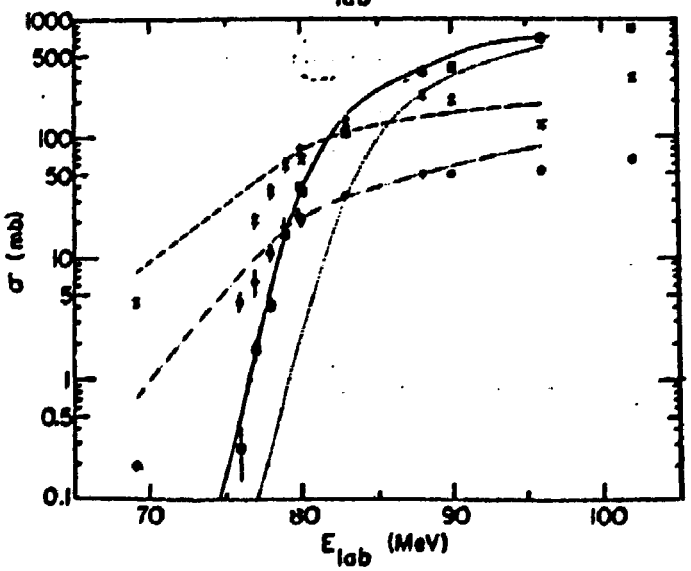

b)

Fig. 11

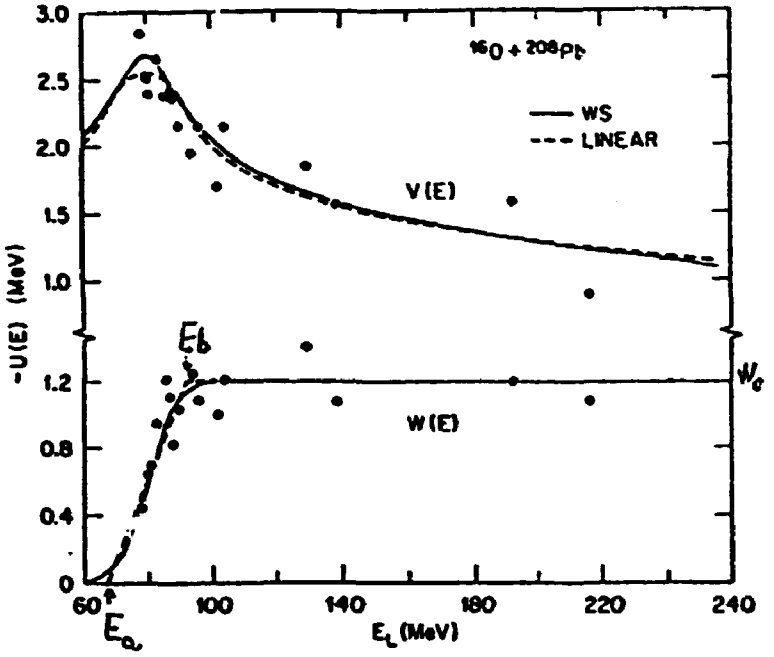
a)
$^{16}O + ^{208}Pb$
WS
LINEAR
V(E)
W(E)
E_b
W_0
E_0
-U(E) (MeV)
E_L (MeV)
3.0
2.5
2.0
1.5
1.0
1.2
0.8
0.4
0
60
100
140
180
220
240

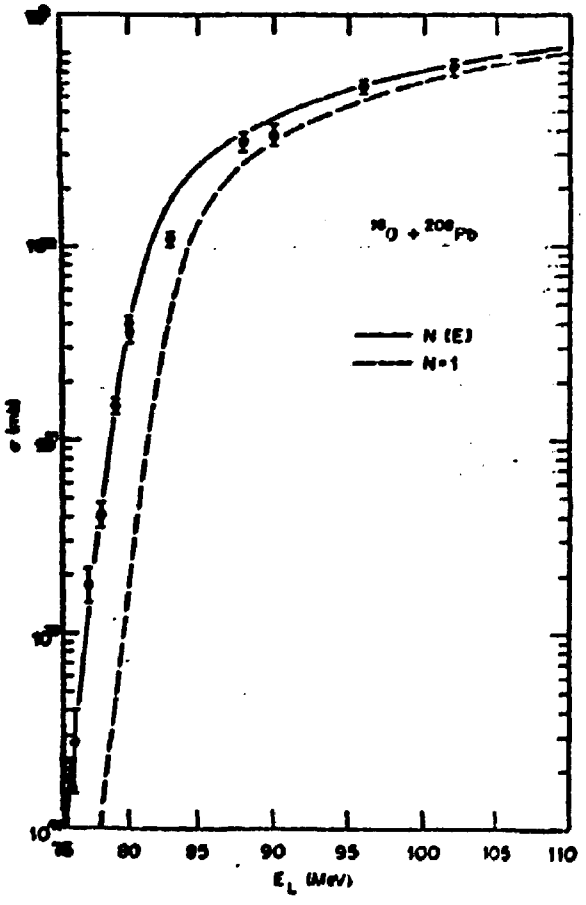
b)
$^{16}O + ^{208}Pb$
N (E)
N=1
80
85
90
95
100
105
110
E_L (MeV)

Fig. 12

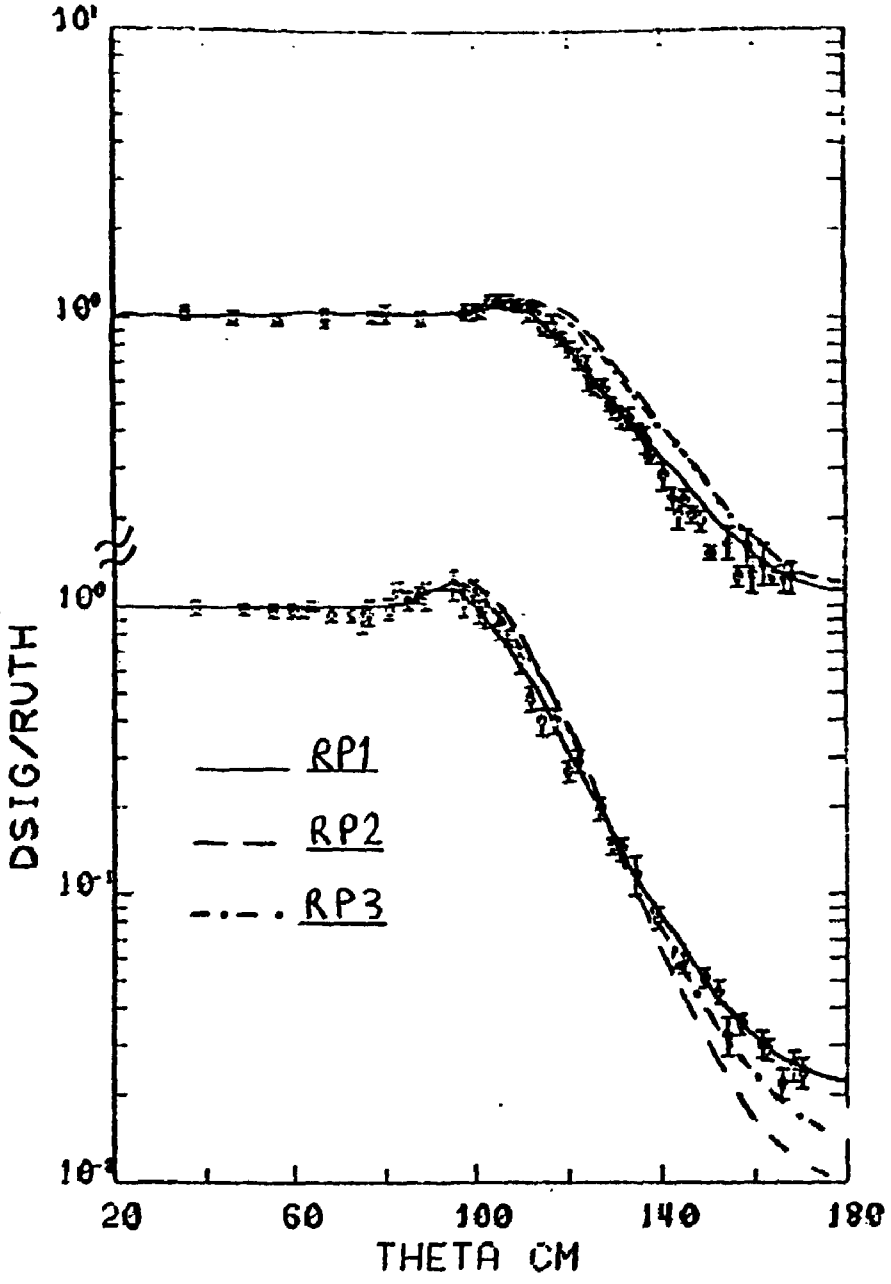

Fig. 13

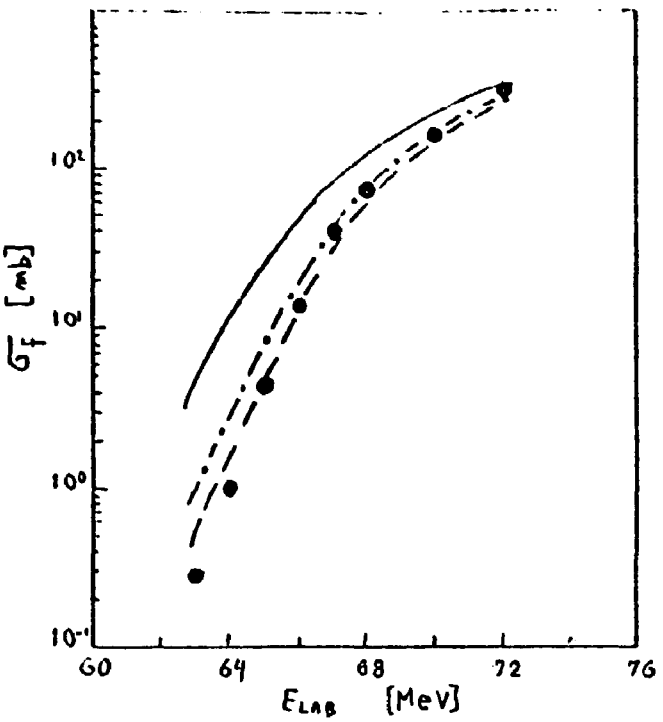
σ_f [mb]
10^2
10^1
10^0
10^{-1}
60
64
68
72
76
E_{LAB} [MeV]

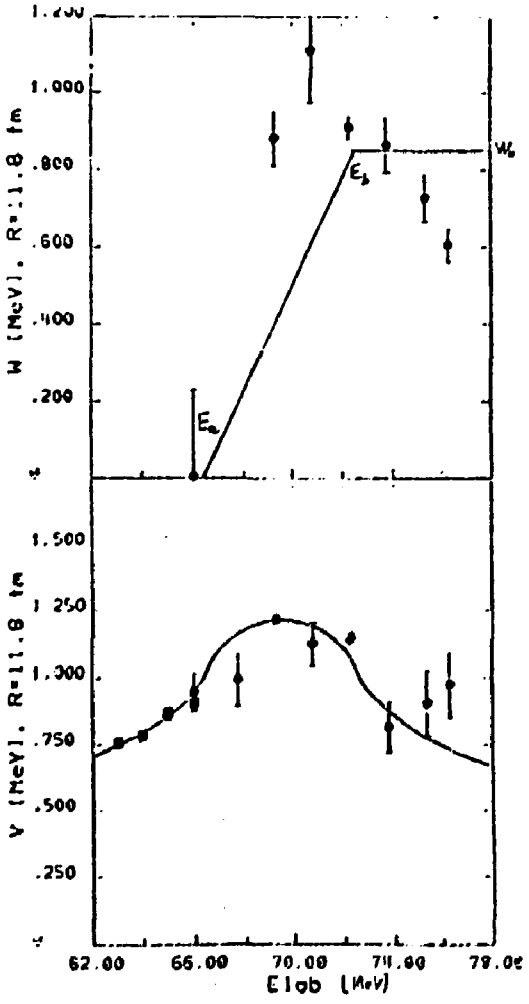
W [MeV], R=1.8 fm
1.000
.800
.600
.400
.200
W_0
E_b
E_a
V [MeV], R=11.8 fm
1.500
1.250
1.000
.750
.500
.250
62.00
66.00
70.00
74.00
78.00
Elab (MeV)

Fig. 15